



## Full length article

# Determining grain boundary energies from triple junction geometries without discretizing the five-parameter space

Yu-Feng Shen <sup>a</sup>, Xiaoting Zhong <sup>b</sup>, He Liu <sup>a</sup>, Robert M. Suter <sup>a</sup>, Adam Morawiec <sup>c</sup>, Gregory S. Rohrer <sup>b,\*</sup>

<sup>a</sup> Carnegie Mellon University, Department of Physics, Pittsburgh, PA, 15213, USA

<sup>b</sup> Carnegie Mellon University, Department of Materials Science and Engineering, Pittsburgh, PA, 15213, USA

<sup>c</sup> Polish Academy of Sciences, Institute of Metallurgy and Materials Science, Reymonta 25, 30-059, Krakow, Poland

## ARTICLE INFO

## Article history:

Received 28 September 2018

Received in revised form

8 December 2018

Accepted 11 December 2018

Available online 14 December 2018

## Keywords:

Polycrystalline material

Grain boundary energy

Triple junction geometry

Five-parameter space

Regularization

## ABSTRACT

Grain boundary energy anisotropy plays an important role in many science and engineering problems. This paper presents a new numerical method for determining the grain boundary energy distribution (GBED) from the microstructures of polycrystalline materials. The method assumes that triple junctions are in local equilibrium, that this equilibrium is described by the Herring equation, and can be expressed using the Hoffman-Cahn formalism of the capillarity vector. The conventional method discretizes the five-parameter space and then fits the energy for each discrete bin. The new method minimizes the difference between similar boundaries in the dataset while obeying the equilibrium equation at triple junctions. This non-parametric approach shows smaller error than the conventional method, and it can also determine the grain boundary energies from datasets that have small numbers of triple junctions if their configurations are clustered in the five-parameter space, which is not possible using the conventional method. In addition, the proposed non-parametric approach performs better when the number of triple junctions increases, which is not always true for the conventional method.

© 2018 Acta Materialia Inc. Published by Elsevier Ltd. All rights reserved.

## 1. Introduction

### 1.1. Background

The property and performance of polycrystalline materials can be modified by engineering the grain boundary network [1]. For example, Kokawa shows a one-step thermomechanical process can suppress the weld-decay of an austenitic steel as the degree of sensitization drops 63% and the corrosion rate drops 44% [2]. It was shown that the steady state creep rate of Ni-16Cr-9Fe decreases 96% at 360°C in an argon atmosphere as the fraction of coincident site lattice boundaries increases from 16% to 43% [3]. Underlying such dramatic performance changes is the fact that grain boundary properties are anisotropic. This paper focuses on determining the relative grain boundary energies, which govern the evolution of the grain boundary network at high temperatures.

Decades of research have been devoted to finding a concise and

descriptive function for the dependence of the grain boundary energy on the five crystallographic parameters. Several theoretical models [4–8] are inspired by experimental observations [9–12]. However, though the existing models usually work well under their specific set of assumptions, most of them fail to capture the entire grain boundary energy landscape [13]. The greatest obstacles are the vast number of distinct grain boundary types and limited experimental data. Recently, Bulatov proposed an interpolation function which appears to successfully capture variations of grain boundary energy in face-centered cubic materials for the first time [13]. Nevertheless, Bulatov's function was entirely based on the Read-Shockley-Wolf function [14] and 388 grain boundary energies calculated by molecular dynamics simulations [15]. It is likely that if more accurate and abundant experimental data becomes available, it will be possible to create a similar, or more general, experiment-based grain boundary energy function.

A method to extract relative grain boundary energies from experimental data was described by Morawiec in 2000 [16]. The experimental data used as input for the method consists of the geometries of many triple lines; for each triple line, the three grain orientations, the triple line direction, and the orientations of the

\* Corresponding author.

E-mail address: [gr20@andrew.cmu.edu](mailto:gr20@andrew.cmu.edu) (G.S. Rohrer).

three grain boundary planes are specified. The method has been used to reconstruct the grain boundary energy distributions of MgO, Ni, Y<sub>2</sub>O<sub>3</sub>, austenite, and ferrite [17–21].

## 1.2. Preliminaries

Grain boundaries can be characterized by five macroscopic parameters. Typically, three parameters are used for the lattice misorientation across the boundary and the other two for the boundary plane orientation [22]. Experimental systems provide voxel-wise orientations in a 3D volume, which can be used to determine grain orientations and boundary plane inclinations. Using the same notation as in Ref. [16], the orientations of the two neighboring grains are represented by two special orthogonal matrices  $\bar{\mathbf{o}}_1$  and  $\bar{\mathbf{o}}_2$  (the over-line means that the variable is in the sample frame, otherwise the variable is in the crystal frame). So the misorientation is  $\mathbf{m} = \bar{\mathbf{o}}_1 \bar{\mathbf{o}}_2^T$ , and the normal direction of the boundary directed from the first grain to the second grain is represented by a unit vector  $\mathbf{n}$ . The macro-parameters  $\mathbf{m}$  and  $\mathbf{n}$  together will determine the grain boundary energy  $\gamma$ . For convenience, we can use a  $4 \times 4$  matrix  $\mathbf{b}$  to represent all five parameters:

$$\mathbf{b}(\mathbf{m}, \mathbf{n}) = \begin{bmatrix} \mathbf{m} & \mathbf{n} \\ -\mathbf{n}^T \mathbf{m} & 0 \end{bmatrix}.$$

As a result of crystal symmetry, there are many distinct sets of parameters corresponding to physically indistinguishable grain boundaries. A  $4 \times 4$  matrix

$$\mathbf{C}_i = \begin{bmatrix} \mathbf{c}_i & 0 \\ 0 & 1 \end{bmatrix},$$

where  $\mathbf{c}_i$  is a  $3 \times 3$  matrix used to represent one of the symmetry operations of the crystal point group (without improper rotations). Then, the set of physically identical grain boundaries of  $\mathbf{b}$  consists of  $\mathbf{C}_i \mathbf{b} \mathbf{C}_j$ ,  $\mathbf{C}_i \mathbf{b}^T \mathbf{C}_j$ ,  $\mathbf{C}_i \mathbf{b}^- \mathbf{C}_j$ ,  $\mathbf{C}_i (\mathbf{b}^-)^T \mathbf{C}_j$ , where  $\mathbf{b}^- = \mathbf{b}(\mathbf{m}, -\mathbf{n})$ . We use  $S_q(\mathbf{b})$  as the  $q$ th element in this set. Obviously, all elements in this set have the same energy because they are physically identical.

It is convenient to define the “distance” between boundaries  $i$  and  $j$  as  $\chi^2 = \chi_{ij}^2 = \min_q \|S_q(\mathbf{b}_i) - \mathbf{b}_j\|^2/2$ , where the norm  $\|\cdot\|$  of a matrix  $\mathbf{M}$  is given by  $\|\mathbf{M}\| = \text{tr}(\mathbf{M}^T \mathbf{M})^{1/2}$ . The exceptional case is the distance from the “no misorientation boundary”  $\mathbf{b}(\mathbf{I}_3, \mathbf{n})$ , where  $\mathbf{I}_3$  is the identity matrix. Since the normal direction is irrelevant when there is no misorientation between grains, in this case we define  $\chi^2 = \min_q \|S_q(\mathbf{m}) - \mathbf{I}_3\|^2/2$ , where  $\mathbf{m}$  is the  $3 \times 3$  misorientation for boundary  $\mathbf{b}(\mathbf{m}, \mathbf{n})$  and  $S_q(\mathbf{m})$  are the misorientations symmetrically equivalent to  $\mathbf{m}$ , i.e.,  $\mathbf{c}_i \mathbf{m} \mathbf{c}_j$  and  $\mathbf{c}_i \mathbf{m}^T \mathbf{c}_j$  for all  $\mathbf{c}_i, \mathbf{c}_j$ .

The grain boundary energy  $\gamma(\mathbf{b}) = \gamma(S_q(\mathbf{b}))$  is what we want to infer from experimental data. Based on the assumption of local equilibrium, we can recover relative grain boundary energies from the triple junction geometries.

For the triple junction that consists of grain boundaries  $i, j, k$ , the equilibrium equation is

$$(\bar{\xi}_i + \bar{\xi}_j + \bar{\xi}_k) \times \bar{\mathbf{t}} = 0, \quad (1)$$

where  $\bar{\mathbf{t}}$  is tangent to the junction and  $\bar{\xi}_i$  is the capillarity vector of the  $i$ th boundary. The capillarity vector is defined as

$$\xi = \gamma \mathbf{n} + \frac{\partial \gamma}{\partial \mathbf{n}}.$$

For more details on the capillarity vector, readers are referred to the original papers [23–25].

## 1.3. Conventional method

We refer to Morawiec’s method [16] as the conventional method in this paper. In the conventional method, the five-parameter space is divided into discrete bins and each bin is associated with one unknown capillarity vector  $\xi_\alpha$  (we use Greek letters as the indices of the bins). For every grain boundary in the experimental dataset, its capillarity vector  $\bar{\xi}_i$  is calculated by averaging all the capillarity vectors  $\xi_\alpha$  of the bins that contain  $\mathbf{b}_i$ ’s equivalences. Substituting the  $\bar{\xi}_i$ ’s in Eq. (1) with linear combinations of  $\xi_\alpha$ ’s for all triple junctions yields a set of linear equations for  $\xi_\alpha$ ’s

$$\mathbf{A} \cdot \mathbf{X} = \mathbf{0}, \quad (2)$$

where  $\mathbf{X} = [\xi_1^x \ \xi_1^y \ \xi_1^z \ \dots \ \xi_\alpha^x \ \xi_\alpha^y \ \xi_\alpha^z \ \dots \ \xi_M^x \ \xi_M^y \ \xi_M^z]^T$ ,  $M$  is the total number of bins,  $\xi_\alpha^x, \xi_\alpha^y, \xi_\alpha^z$  are the  $x, y, z$  components of  $\xi_\alpha$ , and matrix  $\mathbf{A}$  is derived from the equilibrium equations and the symmetry operations. See Ref. [16] for the detailed expression of matrix  $\mathbf{A}$ . Finally, we solve for the  $\xi_\alpha$ ’s from this linear equation set by minimizing the sum of squared residuals while keeping the norm of the vector of unknowns. The solution is the eigenvector corresponding to the smallest eigenvalue of  $\mathbf{A}^T \mathbf{A}$ . It can be solved by gradient-based iterative methods.

So, mathematically, this method uses a set of basis functions (having value 1 in one bin and value 0 in other bins) for the capillarity vector function  $\xi(\mathbf{b})$ , and all the capillarity vectors,  $\xi_\alpha$ , defined on the bins are the coefficients. The reconstruction process is to find the best set of coefficients to approximate a  $\xi(\mathbf{b})$  that satisfies all the equilibrium equations. When the grain boundary parameters are discretized, the three Eulerian angles giving the disorientation are considered within the domain of 0 to 90°. For the spherical angles defining the boundary inclination, the polar angle is also considered within the domain of 0 to 90° and the azimuthal angle is considered within the domain of 0 to 360°. Using a typical discretization with 10° bins, there are  $M = 9^4 \times 36$  bins and  $3M = 708588$  coefficients to be fit [26,27].

Currently, a typical 3D microstructure dataset measured by electron backscatter diffraction (EBSD) [28] or high energy X-ray diffraction microscopy (HEDM) [29] contains  $10^4 \sim 10^5$  triple junctions [20,21], and each triple junction gives one equilibrium equation (Equation (1)), which corresponds to two independent scalar equations. So the reconstruction problem is an under-determined inverse problem, which has more unknowns (708588) than equations, i.e.  $\mathbf{A}$  in equation (2) has more columns than rows, so  $\mathbf{A}^T \mathbf{A}$  has multiple eigenvectors corresponding to the smallest eigenvalue 0. In the original paper [16], the author addressed this issue by setting the starting point to be the boundary normal unit vector (i.e.  $\xi_{\alpha 0} = \mathbf{n}_\alpha$ ) and using the gradient descent algorithm to find the minimum. Empirically this works very well for most cases, and the reconstructed grain boundary functions are consistent with theoretical expectations [17–21].

## 1.4. Motivation

While the conventional approach has been useful, it also has a number of limitations:

- It can not take advantage of increasing dataset size. If the dataset is too large, the discretization of five-parameter space can lead to some unexpected artifacts. See Section 4.3 for details.
- In many samples, grain boundaries are not distributed uniformly in the five-parameter space and in some cases, they are concentrated in a small region of five-parameter space and we only want to get the grain boundary energy function in that

region. The conventional method cannot determine grain boundary energies from this kind of dataset easily. See Section 4.2 for details.

In this paper, we propose a new framework for determining grain boundary energies from triple junction geometry. Instead of discretizing the five-parameter space and fitting the coefficients, this approach directly fits the capillarity vector  $\xi_i$  of each grain boundary in the dataset. Because the proposed approach does not use any parametric model for the grain boundary energy function, we refer to it as the non-parametric reconstruction method. The reconstruction method is described in detail in Section 2, and some results reconstructed from simulated triple junction geometries are presented in Section 4.

## 2. Non-parametric reconstruction framework

The goal of our new approach is to reconstruct the capillarity vector  $\xi_i$  of each grain boundary in the dataset without discretizing the five-parameter space. The unknowns can be written as a vector

$$\mathbf{X} = \left[ \xi_1^x \xi_1^y \xi_1^z \dots \xi_i^x \xi_i^y \xi_i^z \dots \xi_{3W}^x \xi_{3W}^y \xi_{3W}^z \right]^T,$$

where  $W$  is the total number of triple junctions and the number of unknowns is  $9W$  (three capillarity vectors for each triple junction, and three components for each vector).

We define  $S(J)$  as the set of grain boundary IDs that consist in triple junction  $J$ , whose equilibrium equation (Eq. (1)) can be written as

$$0 = \sum_{i \in S(J)} \sum_l B_{j,a^i}^{i,l} \xi_i^l,$$

where  $B_{j,a}^{i,l} \equiv \sum_{b,c} \varepsilon_{abc} \bar{o}_i^{bc}$  and  $\varepsilon_{abc}$  is the permutation symbol. See Appendix A for details.

Using the subscript  $(j, a)$  as the row index, and the superscript  $(i, l)$  as the column index of matrix  $\mathbf{B}$ , we have a matrix equation  $\mathbf{B} \cdot \mathbf{X} = \mathbf{0}$  to represent the equilibrium equations of all the triple junctions. There are  $3W$  equations, and only  $2W$  of them are independent, so this reconstruction problem is also an under-determined inverse problem. Because of this, some regularization techniques are needed. Mathematically, we can write it as a constrained minimization problem:

$$\begin{aligned} \min_{\mathbf{X}} R(\mathbf{X}) \\ \text{s.t. } \|\mathbf{X}\|^2 = 1, \quad \mathbf{B} \cdot \mathbf{X} = \mathbf{0}. \end{aligned} \quad (3)$$

There are many choices for the regularization term  $R(\mathbf{X})$ . A common choice is based on the assumption that grain boundary energy functions are smooth, which means that if two grain boundaries  $i$  and  $j$  have similar physical characteristics (i.e.,  $\chi_{ij}$  is small), then their capillarity vectors should be similar, i.e.,

$$R(\mathbf{X}) = \sum_{(i,j) \in E} w_{ij} \|\xi_i - \mathbf{T}_{ij} \cdot \xi_j\|^2, \quad (4)$$

where  $E = \{(i, j) \mid \text{boundary } i \text{ and } j \text{ are similar}\}$ ,  $w_{ij}$  is the weight that is proportional to the similarity of boundaries  $i$  and  $j$ , and  $\mathbf{T}_{ij}$  is the operator that makes boundaries  $i$  and  $j$  have similar plane normal directions, i.e.,  $\mathbf{T}_{ij} \mathbf{n}_j \approx \mathbf{n}_i$ . Appendix A shows how to

calculate  $\mathbf{T}_{ij}$  from the symmetry operator and the misorientation. This regularization term penalizes the difference between capillarity vectors of physically similar grain boundaries. The form of the weight  $w_{ij}$  and the criterion for including a pair of boundaries in the set  $E$  are essential in this non-parametric framework. In this paper, the set  $E$  contains the boundary pairs whose distances are smaller than a threshold, and we use the inverse of distance as the weight  $w_{ij} = 1/\chi_{ij}$ . See Appendix A for more details.

Other regularization terms are also possible in this framework, for example using “similar energy” instead of “similar capillarity vector”. Different choices correspond to different prior knowledge of the grain boundary energy distribution (GBED) and they will influence the results, robustness, and efficiency of the reconstruction. One thing we need to emphasize is that, no matter which regularization term we chose, the reconstruction result always satisfies all the equilibrium equations. The comparison of different regularization terms is beyond the scope of this paper; in the following sections, we will use Eq. (4) as the regularization term.

There are many methods to solve this constrained minimization problem. In this paper, we convert it into an approximate eigenvalue problem and then find the eigenvector corresponding to the smallest eigenvalue (see Appendix A for more details). Once the capillarity vectors are reconstructed, the grain boundary energy is  $\gamma_i = \xi_i \cdot \mathbf{n}_i$ . Based on the values  $\gamma_i$ , the landscape of grain boundary energy function can be constructed by any interpolation method.

### 2.1. Optimization method

Both the conventional method and the non-parametric approach make it necessary to solve a minimization problem. The projected gradient descent method was used in the prior work [16]. In this paper, we rephrase the minimization problems as eigenvalue problems, which can be solved efficiently by the Locally Optimal Block Preconditioned Conjugate Gradient (LOBPCG) method [30]. It is also an iterative method but uses more information besides the gradient. A comparison between several different optimization methods was made. In Fig. 1, the LOBPCG method converges much faster than other two methods. Faster optimization methods not only make it possible to reconstruct larger datasets, they also allow for more extensive investigation of the performance of the reconstruction under varying conditions.

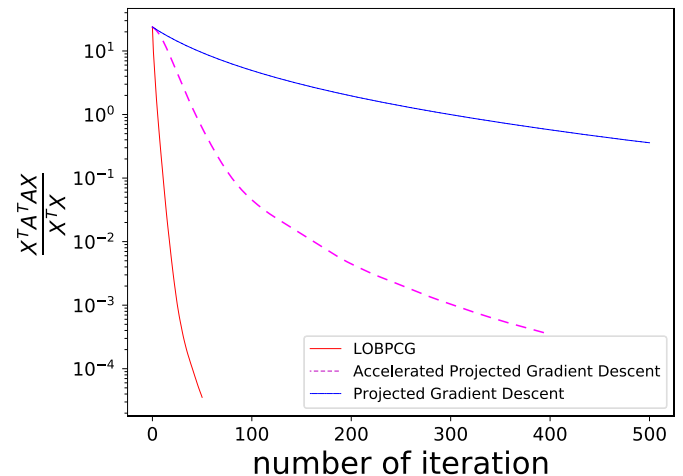


Fig. 1. Comparison of convergence rate of different optimization methods. Projected Gradient Descent, Accelerated Projected Gradient Descent, and LOBPCG were used for the same problem. LOBPCG outperforms the other two methods.

### 3. Simulated datasets

We tested the non-parametric method and the conventional method on several simulated datasets, which are only collections of triple junction geometries instead of the whole 3D microstructures. Based on any user-defined grain boundary energy functions, the simulation code can calculate the capillarity vector for any grain boundary parameters, and it randomly generates the triple junction geometries that satisfy the equilibrium equations. The details of the simulation are in the Appendix of [16].

#### 3.1. Model grain boundary energy function

In this paper, the grain boundary energy functions that were used to create simulated triple junction geometries are based on a uniform energy distribution with superimposed cusps. The cusps are shaped in analogy to the Read-Shockley model [4]:

$$f(x, a) = ax(1 - \ln x) + (1 - a) \text{ for } 0 < x \leq 1$$

$$f(0, a) = 1 - a \text{ and } f(x, a) = 1 \text{ otherwise,}$$

where  $a$  determines the “depth” of the cusp and  $x$  is the “relative distance” from the cusp center. For the model that has cusps at  $\mathbf{b}_k$  ( $k = 1, 2, 3, \dots$ ), the grain boundary energy is  $\gamma(\mathbf{b}) = \prod_k f(\chi(\mathbf{b}, \mathbf{b}_k)/w_k, a_k)$  where  $w_k, a_k$  are the width and depth of cusp  $k$ . The distance  $\chi$  is defined in Section 1.2. So, the grain boundary energy is unity everywhere outside the cusps, and the cusps have the shape of the Read-Shockley expression.

#### 3.2. Datasets

We used two hypothetical grain boundary energy functions, whose cusps are listed in Table 1. The depth of each cusp is  $1/\sqrt{\Sigma}$  and the width is  $\pi/(12\sqrt{\Sigma})$ .

Model A has eight cusps and their  $\Sigma$ s are the unit cell volume of the coincidence site lattice (CSL) in units of the elementary unit cell volume. Based on model A, we generated a dataset containing 260000 random triple junctions, which we refer to as **DA26**. The grain boundaries in **DA26** are nearly uniformly distributed in the five-parameter space. We refer to the first 60000 triple junctions in **DA26** as **DA06**, which is close to the size of a real experimental dataset.

Model B mimics a sample with ideal axial texture and a columnar microstructure. It has 2 cusps, one is zero misorientation ( $\Sigma = 1$ ), and the other one is manually picked whose  $\Sigma$  is just used in the simulation code for calculating the depth and width but is not related to the inverse coincidence. Using model B, we generated

**Table 1**

Cusps in our grain boundary energy function models. We used  $1/\sqrt{\Sigma}$  as the depth of the cusp and  $\pi/(12\sqrt{\Sigma})$  as the width of cusp.

Model	$\Sigma$	misorientation		boundary
		angle (°)	axis	plane
A	1	0.00	N/A	N/A
	3	60.00	[1 1 1]	(1 1 1)
	5	36.87	[1 0 0]	(0 2 1)
	7	38.21	[1 1 1]	(1 2 $\bar{3}$ )
	9	38.94	[1 1 0]	(1 $\bar{1}$ 2)
	11	50.48	[1 1 0]	(2 $\bar{2}$ 3)
	13	22.62	[1 0 0]	(0 3 2)
	13	27.80	[1 1 1]	(1 3 $\bar{4}$ )
B	1	0.00	N/A	N/A
	2	20.00	[0 0 1]	(1 1 0)

a dataset containing 1538 triple junctions, which we refer to as **DB**. The grain boundaries in **DB** are constrained in a 2D subspace of the five-parameter space: all misorientation axes are [0 0 1] and all boundary normals are perpendicular to [0 0 1]. In other words, in this dataset, all grains' [0 0 1] directions are parallel to a same direction, and that direction is also parallel to all junctions. Model B's cusps were chosen in this 2D subspace deliberately.

### 4. Results

Because Eq. (1) is homogeneous, all grain boundary energies can only be determined up to a constant factor. To compare with the ground truth, we normalize the reconstructed grain boundary energies so that the average energy is the same as the average energy of the ground truth distribution; we refer to these as “normalized energies,”  $\gamma_{rec} \cdot \gamma_{rec}$  then has whatever units are used to define the ground truth dataset.

#### 4.1. Results on a normal size dataset

The performance of the reconstruction on **DA06** is representative of real datasets. Fig. 2 shows the GBED for the  $\Sigma 7$  misorientation of **DA06**, the stereographic projections are generated by a method based on boundary-space metrics [27]. Fig. 3 demonstrates the energies of grain boundaries that are inside of  $\Sigma 1$  cusp. Both the conventional method and the non-parametric method reconstructed the grain boundary energies well.

Fig. 4 shows the reconstruction error in more detail. For every grain boundary (GB), we calculate the difference between normalized reconstructed energy and the ground truth  $\gamma_{rec} - \gamma_{true}$ , which have zero mean over the whole dataset by the definition of  $\gamma_{rec}$ . However, after we bin the grain boundaries by their true energy  $\gamma_{true}$ , the averaged  $\gamma_{rec} - \gamma_{true}$  for each bin is no longer zero. As shown in Fig. 4 (a), grain boundaries with smaller  $\gamma_{true}$  tend to have larger  $\gamma_{rec} - \gamma_{true}$ , which means the cusps in the grain boundary energy function are smoothed by the reconstruction. Fig. 4(b) and (c) are the detailed  $\gamma_{rec} - \gamma_{true}$  distributions in the bins  $0.45 < \gamma_{true} < 0.6$  and  $0.75 < \gamma_{true} < 0.9$ , respectively. As we can see, the non-parametric method results have smaller bias and variance than the conventional method in almost every bin.

#### 4.2. Results on a clustered dataset

Sometimes in real materials grain boundaries are not uniformly distributed in the five-parameter space. For example, the data will be clustered in a textured sample, and we may want to reconstruct the energy of grain boundaries in those datasets. In these cases, we actually only need the grain boundary energy function values in constrained regions of the five-parameter space. While the

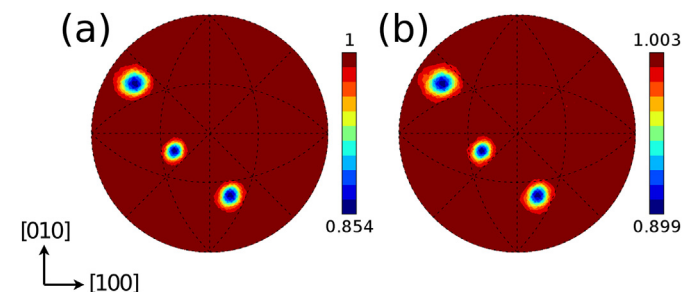


**Fig. 2.** Stereographic projections of the normalized grain boundary energy distribution (GBED) for the  $\Sigma 7$  misorientation of **DA06**. (a) Ground truth; (b) reconstructed by the non-parametric method.

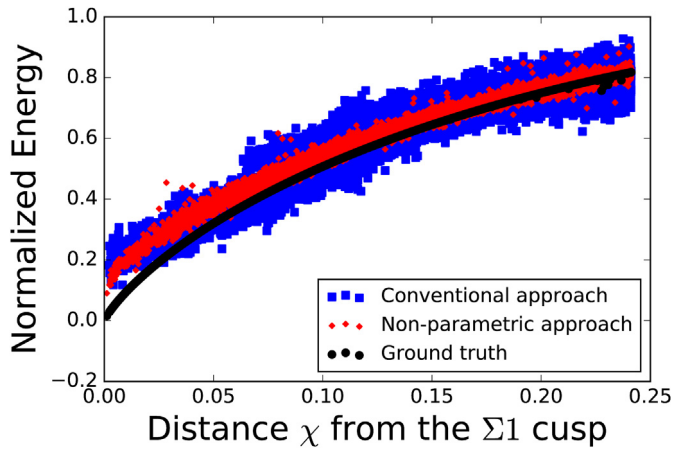


**Fig. 3.** Comparison of the conventional method and the non-parametric method reconstruction results near the  $\Sigma 1$  cusp of **DA06**. The distance  $\chi$  is defined in Section 1.2. Every point represents one grain boundary, blue points are results of the conventional approach, red points are results of the non-parametric approach, and the ground truth are represented by black points. Reconstructed energies have been normalized so that they have the same average value as the ground truth distribution. (For interpretation of the references to colour in this figure legend, the reader is referred to the Web version of this article.)

conventional method still tries to reconstruct the grain boundary energy function on the whole five-parameter space, the non-parametric approach inherently exploits the clustered structure in the datasets. Therefore, we can expect that the non-parametric approach can use less data but get a better reconstruction result than the conventional method.

Dataset **DB** is an extreme case of a clustered dataset with all grain boundaries located in a 2D subspace of the five-parameter space. We tested both the conventional method and the non-parametric method on this dataset, and the reconstructed energies are shown in Fig. 5. In Fig. 5, all grain boundaries are ordered by their true energy  $\gamma_{true}$  so that smaller grain ID corresponds to lower  $\gamma_{true}$ . We can see that the non-parametric method can reconstruct the energies of **DB** fairly well. Fig. 6 shows the mean value and standard deviation of the difference between reconstructed energy and the ground truth  $\gamma_{rec} - \gamma_{true}$  for grain boundaries with different  $\gamma_{true}$ .

#### 4.3. Effects of the dataset size

It is important to know how dataset size influences the reconstruction's performance. To investigate this, we reconstructed the grain boundary energies using only the first  $k \times 10^4$  triple junctions in **DA26**, where  $k = 1, 3, 6, 12, 14, 16, 17, 18,$  and 26. The reconstruction results on these subsets are shown in Fig. 7. Because the reconstruction errors are different for the cusp and the remaining region, we separated the grain boundaries into two categories,  $\gamma_{true} > 0.9$  and  $\gamma_{true} < 0.9$ , which correspond to the grain

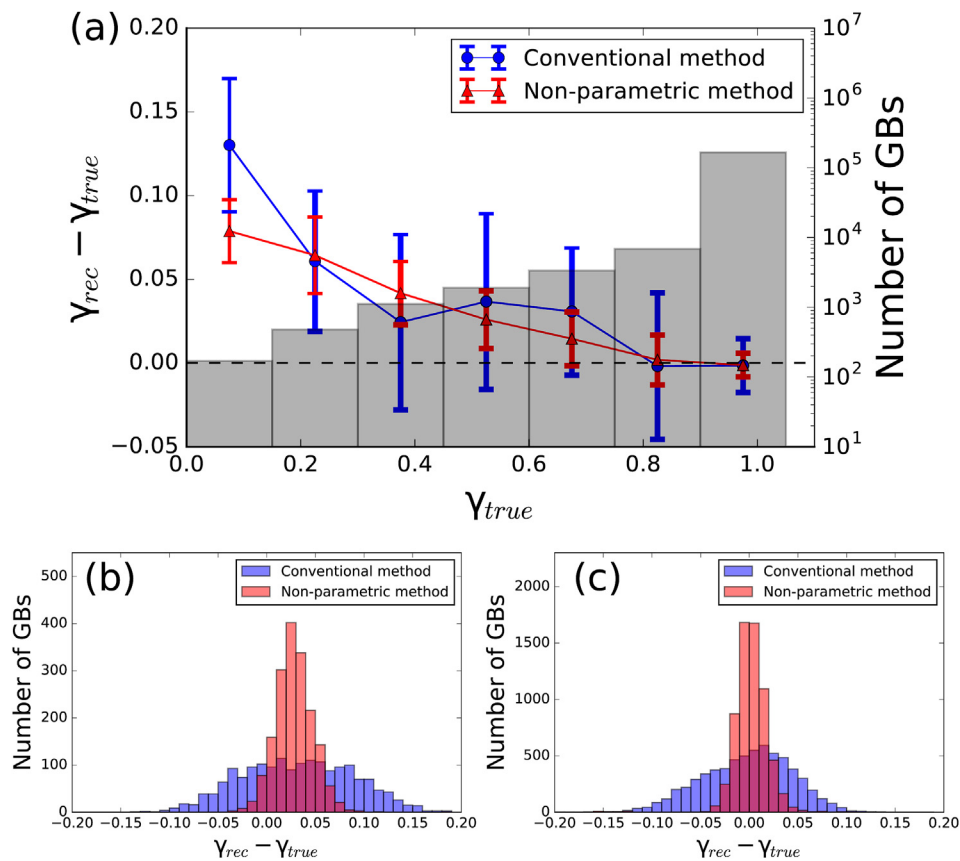


**Fig. 4.** Reconstruction results of the conventional method and the non-parametric method on **DA06**. We calculated the difference between reconstructed energy and the ground truth  $\gamma_{rec} - \gamma_{true}$  for every grain boundary. All grain boundaries are binned by their true energy  $\gamma_{true}$ , and for each bin we calculated the mean value and standard deviation of  $\gamma_{rec} - \gamma_{true}$ , which is shown in (a). The gray bars in (a) are the number of grain boundaries in the bins. The histograms in (b) and (c) are the detailed  $\gamma_{rec} - \gamma_{true}$  distributions in the bin  $0.45 < \gamma_{true} < 0.6$  and bin  $0.75 < \gamma_{true} < 0.9$ , respectively. The blue line and bars are results of the conventional method, and the red line and bars are results of the non-parametric method. (For interpretation of the references to colour in this figure legend, the reader is referred to the Web version of this article.)

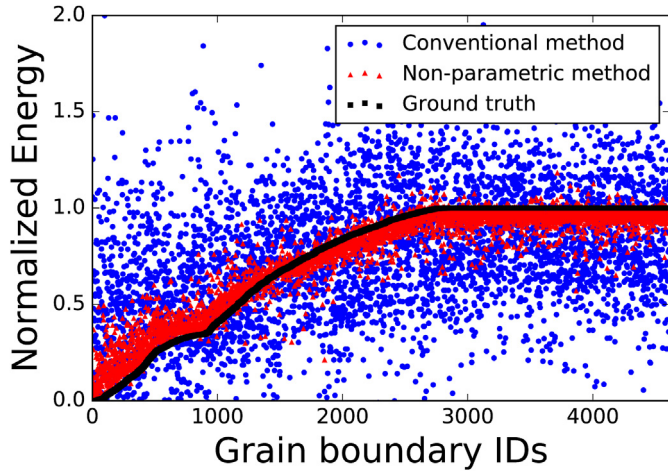


**Fig. 5.** Comparison of the conventional method and the non-parametric method reconstruction results of **DB**. All grain boundaries are ordered by their true energy  $\gamma_{true}$  so that smaller grain ID corresponds to lower  $\gamma_{true}$ . Every point represents one grain boundary, blue points are results of the conventional method, red points are results of the non-parametric method, and the ground truth is represented by black points. Reconstructed energies have been normalized so that they have the same average value as the ground truth distribution. (For interpretation of the references to colour in this figure legend, the reader is referred to the Web version of this article.)

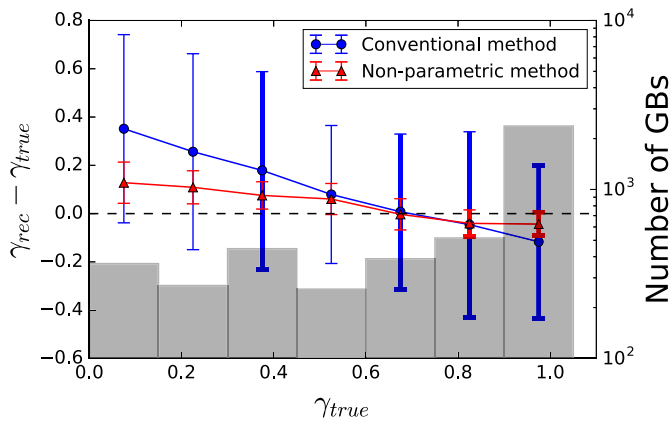


**Fig. 6.** Reconstruction results of the conventional method and the non-parametric method on **DB**. We calculated the difference between reconstructed energy and the ground truth  $\gamma_{rec} - \gamma_{true}$  for every grain boundary. All grain boundaries are binned by their true energy  $\gamma_{true}$ , and for each bin we calculated the mean value and standard deviation of  $\gamma_{rec} - \gamma_{true}$ . The gray bars are the number of grain boundaries in the bins.

boundaries that are outside and inside of the cusps, respectively. The reconstruction error is measured by the square root of mean squared error  $\sqrt{(\gamma_{rec} - \gamma_{true})^2}$ , which includes the effect of bias and variation. As expected, the error of the non-parametric method decreases when the dataset size increases. Surprisingly, the errors in the conventional method are sometimes greater in larger datasets. We will discuss this further in Section 6.

#### 4.4. Effects of measurement noise

Experimental data always has measurement noise. For a microstructure measured by EBSD or HEDM, the uncertainty of grain orientation is negligible, and the main error is the triple junction geometry. To analyze the reconstruction robustness against the error in measuring the triple junction geometry, we artificially added noise to **DA06**. For every triple junctions in **DA06**,

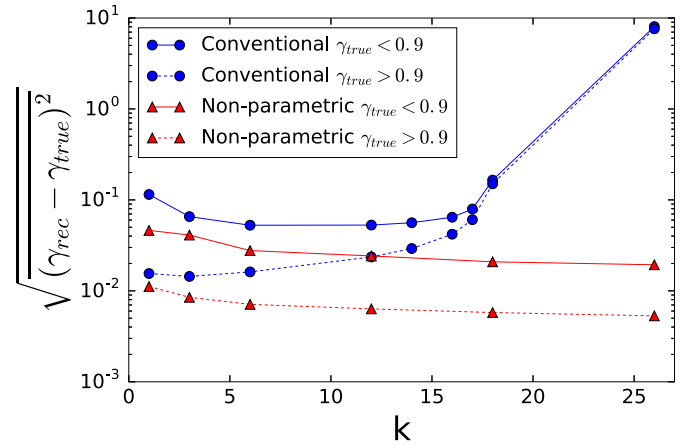


**Fig. 7.** Reconstruction errors using only subsets of **DA26** with different sizes ( $k \times 10^4$ ). Based on the ground truth energies, the grain boundaries in each subset are divided into two categories,  $\gamma_{true} > 0.9$  (dashed line) and  $\gamma_{true} < 0.9$  (solid line), which are outside and inside of cusps, respectively. Blue lines are results of the conventional method, and red lines are results of the non-parametric method. (For interpretation of the references to colour in this figure legend, the reader is referred to the Web version of this article.)

we applied a rotation  $(\delta\phi, \delta\theta, 0)$  to the junction direction, where  $\delta\phi$  and  $\delta\theta$  are randomly generated from a Gaussian distribution with a zero mean. We tested both the conventional method and the non-parametric method on different noisy datasets with different  $\sigma$  (in units of degrees) as the standard deviation of the Gaussian distribution. Fig. 8 demonstrates the reconstruction errors.

### 5. Application to an experimental measurement of MgO

To demonstrate the efficacy of this method for analyzing experimental data, we applied the non-parametric approach to data from an MgO ceramic, originally reported in Ref. [17]. The details of the sample preparation, experimental procedure, and data acquisition can be found in earlier publications [17,31,32]. The three-dimensional orientation data made it possible to determine the geometries of  $1.9 \times 10^4$  triple junctions and these measurements were used as input for the grain boundary energy reconstruction.

In general, the reconstruction errors depend on the energy models. If we assume that the analysis in Section 4.3 and Section 4.4 still hold for the real grain boundary energy function of MgO, then the reconstruction error of normalized grain boundary energy is less than 0.05 because, for this experimental data,  $k = 1.9$  in Fig. 7 and  $\sigma < 10^\circ$  in Fig. 8.

Fig. 9 shows stereographic projections of the reconstructed grain boundary energy distribution (GBED) produced by the new method, the conventional method, and the grain boundary character distribution (GBCD) for MgO for a misorientation of  $5^\circ$  around  $[1\ 1\ 0]$ . The GBCD and GBED were reported in an earlier publication [17]. The GBCD is presented in units of multiples of a random distribution (relative areas). The two grain boundary energy distributions agree in some places. For example, the maximum energy of both distributions is near the position of twist boundaries (marked by circles). However, they disagree at the position of the symmetric tilt boundary (marked by a square), which has a near minimum energy in the GBED produced by the non-parametric method and is a local maximum in the GBED produced by the conventional method. Note that the GBCD has a maximum at the symmetric tilt position. Based on the well-known inverse correlation between the GBED and the GBCD [22], a minimum energy at this position is expected, consistent with the result of the non-parametric method.

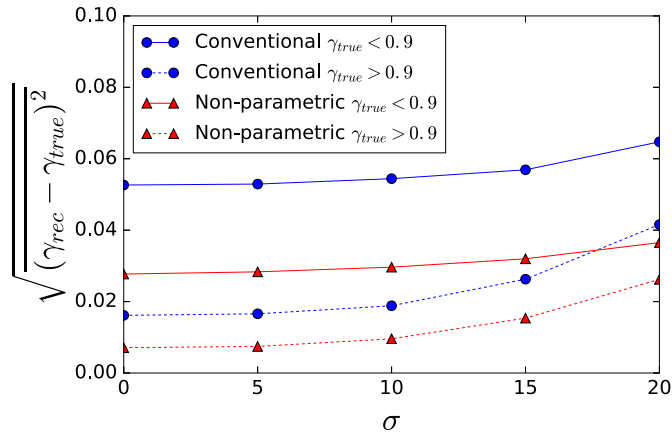


**Fig. 8.** Reconstruction errors of the conventional method and the non-parametric method on the dataset **DA06** with noises of different  $\sigma$  values (in units of degrees), which are the standard deviations of the Gaussian noise that were applied to the triple junction directions. Based on the ground truth energies, the grain boundaries in each dataset are divided into two categories,  $\gamma_{true} > 0.9$  (dashed line) and  $\gamma_{true} < 0.9$  (solid line), which are outside and inside of cusps, respectively. Blue lines are results of the conventional method, and red lines are results of the non-parametric method. (For interpretation of the references to colour in this figure legend, the reader is referred to the Web version of this article.)

## 6. Discussion

We demonstrated in Fig. 4 that both the conventional method and the non-parametric method perform well on a normal size dataset **DA06**. For most grain boundaries, the reconstruction errors are less than 0.1. Cusps are smoothed in the reconstruction, i.e. reconstructed energies of grain boundaries in the cusps are biased to be larger than their true energies. Although the measurement error of triple junction geometries depends on the method of data preprocessing,  $\sigma < 10^\circ$  is a reasonable estimation. As shown in Fig. 8, both methods are robust below this level of noise. For the non-parametric method, the reconstruction error is below 0.04 for grain boundaries inside the cusps and below 0.02 outside the cusps.

An advantage of the non-parametric method over the conventional method is that it utilizes the clustered structure in the datasets, so that it can reconstruct the grain boundary energies of a clustered dataset even if it only contains a small number of triple junctions, which is not possible (without creating a new sub-space for discretization) using the conventional method. As demonstrated by Figs. 5 and 6, the non-parametric method reconstructed the grain boundary energies in **DB** with an error of less than 0.2. Therefore, the energy in that subspace is recovered with reasonable accuracy.

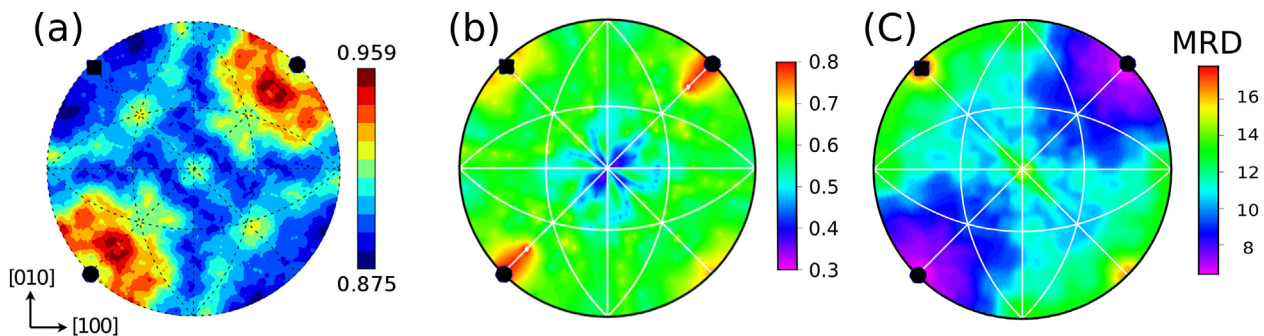


**Fig. 9.** Stereographic projections of the (a) GBED reconstructed using the non-parametric method, (b) GBED reconstructed using the conventional method, and (c) grain boundary character distribution (GBCD) for grain boundaries in MgO with a  $5^\circ$  misorientation around  $[1\ 1\ 0]$ . The GBCD has units of multiples of a random distribution and the GBEDs are normalized energies.

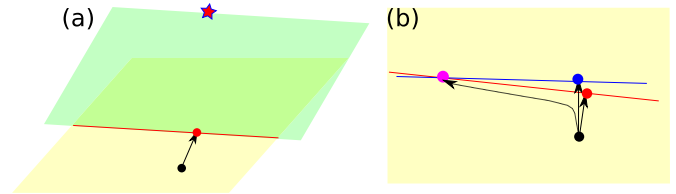


**Fig. 10.** Geometric interpretation. (a) Red star is the true solution, yellow plane is the linear span of the basis functions, green plane is the subspace that satisfies all triple junction equilibrium equations, red line is the overlap of yellow plane and green plane, black dot is the iteration starting point, red dot is the approximated solution found in the yellow plane, which is at the red line and close to the black dot. (b) The yellow plane is the linear span of the basis functions, one set of equilibrium equations constrain the solution on the red line, another set of equations constrain the solution on the blue line, black dot is the iteration starting point. If the dataset only contains the first set of equations, then the approximate solution is at red dot; and if the dataset only contains the second set of equations, then the approximate solution is at blue dot. However, if the dataset contains both, then the approximate solution is at purple dot, which is far away from the true solution. (For interpretation of the references to colour in this figure legend, the reader is referred to the Web version of this article.)

The effect of dataset size is interesting. As shown in Fig. 7, the reconstruction error of the conventional method increases when the number of triple junctions increases in some range. A geometric interpretation is presented in Fig. 10. As we showed above, the conventional method finds the coefficients of a set of basis functions which can span a linear space (yellow plane), and generally the true capillarity vector function (red star) is not in this space, and the solution we find is an approximation (red dot), which satisfies the force balance equations of all the triple junctions. In most cases, the problem is under-determined, so the solution always exists but is not unique. Choosing a good starting point (black dot) for the gradient descent iteration makes the problem converge to a solution (red dot) that can approximate the ground truth (red star). However, if we have more triple junctions, there are more constraints and the solution (purple dot) may not be close to the ground truth anymore.

One way to address this problem is to stop the iterative solution before convergence. The conventional method converges after about 2000 iteration steps for the large size dataset **DA26**. Fig. 11 demonstrates the errors of some intermediate results in the first 200 iteration steps. As we expected,  $\lambda = \|\mathbf{AX}\|^2 / \|\mathbf{X}\|^2$  keeps decreasing, where  $\mathbf{A}$  and  $\mathbf{X}$  are the equation coefficients and variables in Eq. (2). The reconstruction errors decrease in a few iteration steps at first, but increase dramatically after about 150 iteration steps. Therefore, for the dataset **DA26**, if we stop before 150 iteration steps, the reconstruction results will be close to the ground truth. The grain boundary energy distribution (GBED) for the  $\Sigma 11$  misorientation of the intermediate reconstruction is

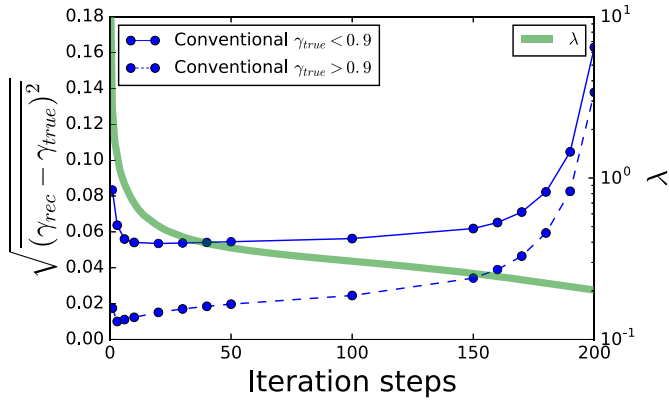


**Fig. 11.** Errors of the intermediate reconstruction results using the conventional method on dataset **DA26**. Based on the ground truth energies, the grain boundaries are divided into two categories,  $\gamma_{true} > 0.9$  (dashed line) and  $\gamma_{true} < 0.9$  (solid line), which are outside and inside of cusps, respectively. The green line is  $\lambda$ , which is defined as  $\|\mathbf{A}\mathbf{X}\|^2/\|\mathbf{X}\|^2$ , where  $\mathbf{A}$  and  $\mathbf{X}$  are the equation coefficients and variables in Eq. (2). (For interpretation of the references to colour in this figure legend, the reader is referred to the Web version of this article.)

shown in Fig. 12. After 10 iterations, the conventional approach shows a GBED that is expected for the  $\Sigma 11$  misorientation. However, it has not converged yet. After 200 steps, the result deviates from the ground truth. So, the number of iterations is an important hyper-parameter for the conventional reconstruction method. The non-parametric approach does not have the same problem as the conventional method, because it does not limit the solution to a subspace. So, as shown in Fig. 7, the reconstruction error of the non-parametric method decreases as the number of triple junctions increases, which is as expected.

Finally, let us note that in this non-parametric framework, the regularization term is based on the “distance” between grain boundaries. The choice of the metric affects the regularization term and, in consequence, the reconstruction results. The definition of grain boundary distance in Section 1.2 follows [16], but other metrics have been discussed in the literature [33–37]. Moreover, with  $1/\chi_{ij}$  as the weight in the regularization term, the singularity at  $\chi_{ij} = 0$  may cause problems on clustered data sets. Testing

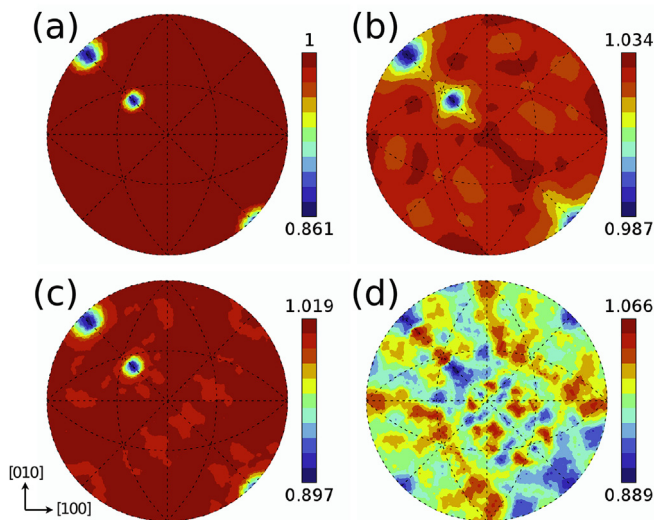


**Fig. 12.** Stereographic projections of the GBED for the  $\Sigma 11$  misorientation at different iteration steps. (a) Ground truth; (b) step 1; (c) step 10; (d) step 200. (b)–(d) are reconstructed by the conventional approach using dataset **DA26**.

alternative metrics and regularization terms for the non-parametric framework will be the subject of future research.

## 7. Conclusions

In this paper, a new framework for reconstructing grain boundary energy from triple junction geometry is demonstrated. This new framework gives good reconstruction results with  $6 \times 10^4$  triple junctions, even when the data are noisy. With more data, the reconstruction results have smaller error. In addition, the performance on a small clustered dataset is also good enough to give information about the grain boundary energy function. Future research will study the performance of the non-parametric reconstruction on different energy function models and with different forms of regularization terms. We will also apply this procedure to several new experimental 3D data sets.

## Acknowledgements

This work was supported by the National Science Foundation of the United States of America under grant DMR-1628994. The authors thank Krzysztof Glowinski for the code used for plotting GBED figures.

## Appendix A. Details of non-parametric approach

### Appendix A.1 Rewriting the equilibrium equation

We define  $S(J)$  as the set of grain boundary IDs that consist in triple junction  $J$ . Vectors and tensors in sample frame are overlined, otherwise they are in crystal frame. Writing all vectors and tensors in component form, the equilibrium equation becomes:

$$\begin{aligned} 0 &= \sum_{b,c} \varepsilon_{abc} \sum_{i \in S(J)} \bar{\xi}_i^b \bar{\xi}_i^c \\ &= \sum_{b,c} \varepsilon_{abc} \bar{\xi}_i^c \sum_{i \in S(J)} (\bar{\mathbf{o}}_i^T \bar{\xi}_i)^b \\ &= \sum_{b,c} \varepsilon_{abc} \bar{\xi}_i^c \sum_{i \in S(J)} \sum_l \bar{o}_i^{bl} \bar{\xi}_i^l \\ \Rightarrow 0 &= \sum_{i \in S(J)} \sum_l B_{J,a}^{i,l} \bar{\xi}_i^l, \end{aligned}$$

$$\text{where } B_{J,a}^{i,l} \equiv \sum_{b,c} \varepsilon_{abc} \bar{\xi}_i^c \bar{o}_i^{lb}.$$

### Appendix A.2 The regularization term

Most of the computation time of the non-parametric approach is spent on constructing the regularization term. Because we need to find “neighbors” for each grain boundary, a naive algorithm has  $O(n^2)$  time complexity, where  $n$  is the total number of grain boundaries in the dataset.

For every grain boundary  $\mathbf{b}$  there are a set of physically identical boundaries  $S_q(\mathbf{b})$ , and they are all related by linear symmetry operators. To compare the capillarity vectors of boundaries  $i$  and  $j$ , we need the operator  $\mathbf{T}_{ij}$  that makes boundaries  $i$  and  $j$  have similar plane normal directions, i.e.,  $\mathbf{T}_{ij} \mathbf{n}_j \approx \mathbf{n}_i$ , which can be calculated as follows:

$$\mathbf{T}_{ij} = \begin{cases} \mathbf{c}_1 & \text{if } S_q(\mathbf{b}_j) = \mathbf{C}_1 \mathbf{b}_j \mathbf{C}_2 \\ -\mathbf{c}_1 \mathbf{m}_j^T & \text{if } S_q(\mathbf{b}_j) = \mathbf{C}_1 \mathbf{b}_j^T \mathbf{C}_2 \\ -\mathbf{c}_1 & \text{if } S_q(\mathbf{b}_j) = \mathbf{C}_1 \mathbf{b}_j^- \mathbf{C}_2 \\ \mathbf{c}_1 \mathbf{m}_j^T & \text{if } S_q(\mathbf{b}_j) = \mathbf{C}_1 (\mathbf{b}_j^-)^T \mathbf{C}_2 \end{cases},$$

where  $q^* = \operatorname{argmin}_q \|\mathbf{b}_i - S_q(\mathbf{b}_j)\|^2$ .

After we find all the neighboring pairs and include them in the set  $E = \{(i, j) \mid \text{boundary } i \text{ and } j \text{ are similar}\}$ , we can construct the regularization term:

$$R(\mathbf{X}) = \sum_{(i,j) \in E} \frac{1}{\chi_{ij}} \|\xi_i - \mathbf{T}_{ij} \cdot \xi_j\|^2,$$

where  $\chi_{ij}$  is the “distance” between boundaries  $i$  and  $j$  defined in Section 1.2. The unknowns are represented by  $\mathbf{X} = [\xi_1^x \ \xi_1^y \ \xi_1^z \ \dots \ \xi_i^x \ \xi_i^y \ \xi_i^z \ \dots \ \xi_{3W}^x \ \xi_{3W}^y \ \xi_{3W}^z]^T$ . In this paper, we use  $E = \{(i, j) \mid \chi_{ij} < 0.03\}$  for **DA06** and  $E = \{(i, j) \mid \chi_{ij} < 0.015\}$  for **DB**, so that most boundaries have more than 30 “neighbors”.

### Appendix A.3 Solving the minimization problem

If we use the equilibrium equations and normalization condition as the constraints, and try to minimize the regularization term, we get the following constrained optimization problem:

$$\min_{\mathbf{X}} \sum_{(i,j) \in E} \frac{1}{\chi_{ij}} \|\xi_i - \mathbf{T}_{ij} \cdot \xi_j\|^2 \equiv \min_{\mathbf{X}} \|\mathbf{C} \cdot \mathbf{X}\|^2$$

$$\text{s.t. } \|\mathbf{X}\|^2 = 1, \quad \mathbf{B} \cdot \mathbf{X} = 0,$$

Where  $\mathbf{C}$  is defined by this regularization term.

One way to solve it is to choose a large enough number  $\lambda$  and the optimization problem approximately becomes:

$$\min_{\mathbf{X}} (\|\mathbf{C} \cdot \mathbf{X}\|^2 + \lambda^2 \|\mathbf{B} \cdot \mathbf{X}\|^2) = \min_{\mathbf{X}} \mathbf{X}^T (\mathbf{C}^T \mathbf{C} + \lambda^2 \mathbf{B}^T \mathbf{B}) \mathbf{X}$$

$$\text{s.t. } \|\mathbf{X}\|^2 = 1.$$

This is again an eigenvalue problem and the eigenvector of  $(\mathbf{C}^T \mathbf{C} + \lambda^2 \mathbf{B}^T \mathbf{B})$  corresponding to smallest eigenvalue can be efficiently computed by LOBPCG method.

Another advantage of introducing  $\lambda$  is that, if the dataset is noisy we may want to relax the equilibrium equation constraints, we can then use smaller  $\lambda$  and have a trade-off between smoothness  $\|\mathbf{C} \cdot \mathbf{X}\|^2$  and the noisy measurements  $\|\mathbf{B} \cdot \mathbf{X}\|^2$ .

### References

- [1] O.K. Johnson, C.A. Schuh, Texture mediated grain boundary network design in three dimensions, *Mech. Mater.* 118 (2018) 94–105.
- [2] H. Kokawa, M. Shimada, M. Michiuchi, Z. Wang, Y. Sato, Arrest of weld-decay in 304 austenitic stainless steel by twin-induced grain boundary engineering, *Acta Mater.* 55 (2007) 5401–5407.
- [3] G.S. Was, V. Thaveprungsriporn, D.C. Crawford, Grain boundary misorientation effects on creep and cracking in Ni-based alloys, *J. Occup. Med.* 50 (1998) 44–49.
- [4] W.T. Read, W. Shockley, Dislocation models of crystal grain boundaries, *Phys. Rev.* 78 (1950) 275.
- [5] M. Ashby, F. Spaepen, S. Williams, The structure of grain boundaries described as a packing of polyhedra, *Acta Metall.* 26 (1978) 1647–1663.
- [6] H. Fecht, H. Gleiter, A lock-in model for the atomic structure of interphase boundaries between metals and ionic crystals, *Acta Metall.* 33 (1985) 557–562.
- [7] D. Wolf, A broken-bond model for grain boundaries in face-centered cubic metals, *J. Appl. Phys.* 68 (1990) 3221–3236.
- [8] D. Wolf, S. Yip, *Materials Interfaces: Atomic-level Structure and Properties*, Springer Science & Business Media, 1992.
- [9] P. Lacombe, N. Yannaquis, La corrosion intercrystalline de la aluminium de haute pureté et ses conséquences au sujet de la nature des joints de grains, *Rev. Metall.* 45 (1948) 68–77.
- [10] G. Wood, W. Stobbs, D.J. Smith, Methods for the measurement of rigid-body displacements at edge-on boundaries using high-resolution electron microscopy, *Philos. Mag.* A 50 (1985) 375–391.
- [11] K. Merkle, D.J. Smith, Atomic structure of symmetric tilt grain boundaries in NiO, *Phys. Rev. Lett.* 59 (1987) 2887.
- [12] K. Merkle, Rigid-body displacement of asymmetric grain boundaries, *Scripta Metall.* (1989) 23.
- [13] V.V. Bulatov, B.W. Reed, M. Kumar, Grain boundary energy function for fcc metals, *Acta Mater.* 65 (2014) 161–175.
- [14] D. Wolf, A Read-Shockley model for high-angle grain boundaries, *Scripta Metall.* 23 (1989) 1713–1718.
- [15] D.L. Olmsted, S.M. Foiles, E.A. Holm, Survey of computed grain boundary properties in face-centered cubic metals: I. grain boundary energy, *Acta Mater.* 57 (2009) 3694–3703.
- [16] A. Morawiec, Method to calculate the grain boundary energy distribution over the space of macroscopic boundary parameters from the geometry of triple junctions, *Acta Mater.* 48 (2000) 3525–3532.
- [17] D.M. Saylor, A. Morawiec, G.S. Rohrer, The relative free energies of grain boundaries in magnesia as a function of five macroscopic parameters, *Acta Mater.* 51 (2003) 3675–3686.
- [18] J. Li, S.J. Dillon, G.S. Rohrer, Relative grain boundary area and energy distributions in nickel, *Acta Mater.* 57 (2009) 4304–4311.
- [19] S.J. Dillon, G.S. Rohrer, Characterization of the grain boundary character and energy distributions of Yttria using automated serial sectioning and EBSD in the FIB, *J. Am. Ceram. Soc.* 92 (2009) 1580–1585.
- [20] H. Beladi, G.S. Rohrer, The relative grain boundary area and energy distributions in a ferritic steel determined from three-dimensional electron backscatter diffraction maps, *Acta Mater.* 61 (2013) 1404–1412.
- [21] H. Beladi, N.T. Nuhfer, G.S. Rohrer, The five-parameter grain boundary character and energy distributions of a fully austenitic high-manganese steel using three dimensional data, *Acta Mater.* 70 (2014) 281–289.
- [22] G.S. Rohrer, Grain boundary energy anisotropy: a review, *J. Mater. Sci.* 46 (2011) 5881.
- [23] C. Herring, Surface tension as a motivation for sintering, *Phys. Powder Metall.* 27 (1951) 143–179.
- [24] D.W. Hoffman, J.W. Cahn, A vector thermodynamics for anisotropic surfaces: I. Fundamentals and application to plane surface junctions, *Surf. Sci.* 31 (1972) 368–388.
- [25] J. Cahn, D. Hoffman, A vector thermodynamics for anisotropic surfaces II. Curved and faceted surfaces, *Acta Metall.* 22 (1974) 1205–1214.
- [26] D.M. Saylor, A. Morawiec, G.S. Rohrer, Distribution of grain boundaries in magnesia as a function of five macroscopic parameters, *Acta Mater.* 51 (2003) 3663–3674.
- [27] K. Glowinski, A. Morawiec, Analysis of experimental grain boundary distributions based on boundary-space metrics, *Metall. Mater. Trans.* 45 (2014) 3189–3194.
- [28] R.A. Schwarzer, D.P. Field, B.L. Adams, M. Kumar, A.J. Schwartz, Present state of electron backscatter diffraction and prospective developments, in: *Electron Backscatter Diffraction in Materials Science*, Springer, 2009, pp. 1–20.
- [29] R. Suter, D. Hennessy, C. Xiao, U. Lienert, Forward modeling method for microstructure reconstruction using X-ray diffraction microscopy: single-crystal verification, *Rev. Sci. Instrum.* 77 (2006) 123905.
- [30] A.V. Knyazev, Toward the optimal preconditioned eigensolver: Locally optimal block preconditioned conjugate gradient method, *SIAM J. Sci. Comput.* 23 (2001) 517–541.
- [31] D.M. Saylor, A. Morawiec, B.L. Adams, G.S. Rohrer, Misorientation dependence of the grain boundary energy in magnesia, *Interface Sci.* 8 (2000) 131–140.
- [32] D.M. Saylor, A. Morawiec, G.S. Rohrer, Distribution of grain boundaries in magnesia as a function of five macroscopic parameters, *Acta Mater.* 51 (2003) 3663–3674.
- [33] J.W. Cahn, J.E. Taylor, Metrics, measures, and parametrizations for grain boundaries: a dialog, *J. Mater. Sci.* 41 (2006) 7669–7674.
- [34] D.L. Olmsted, A new class of metrics for the macroscopic crystallographic space of grain boundaries, *Acta Mater.* 57 (2009) 2793–2799.
- [35] A.P. Sutton, E.P. Banks, A.R. Warwick, The five-dimensional parameter space of grain boundaries, *Proc. Roy. Soc. Lond.: Math. Phys. Eng. Sci.* 471 (2015).
- [36] A. Morawiec, Comment on ‘the five-dimensional parameter space of grain boundaries’ by sutton et al, *Proc. Roy. Soc. Lond.: Math. Phys. Eng. Sci.* 472 (2016).
- [37] A.P. Sutton, Response to commentary by morawiec, *Proc. Roy. Soc. Lond.: Math. Phys. Eng. Sci.* 472 (2016).